



**HAL**  
open science

# Nucleation and growth of carbo-nitride nanoparticles in $\alpha$ -Fe-based alloys and associated interfacial process

Mohamed Gouné, Philippe Maugis, Frédéric Danoix

► **To cite this version:**

Mohamed Gouné, Philippe Maugis, Frédéric Danoix. Nucleation and growth of carbo-nitride nanoparticles in  $\alpha$ -Fe-based alloys and associated interfacial process. *Nanotechnology reviews*, 2015, 4 (6), pp.517-532. 10.1515/ntrev-2015-0032 . hal-01241954

**HAL Id: hal-01241954**

**<https://hal.science/hal-01241954v1>**

Submitted on 12 Jun 2024

**HAL** is a multi-disciplinary open access archive for the deposit and dissemination of scientific research documents, whether they are published or not. The documents may come from teaching and research institutions in France or abroad, or from public or private research centers.

L'archive ouverte pluridisciplinaire **HAL**, est destinée au dépôt et à la diffusion de documents scientifiques de niveau recherche, publiés ou non, émanant des établissements d'enseignement et de recherche français ou étrangers, des laboratoires publics ou privés.



Distributed under a Creative Commons Attribution - NonCommercial - NoDerivatives 4.0 International License

## Review

Mohamed Gouné\*, Philippe Maugis and Frédéric Danoix

# Nucleation and growth of carbo-nitride nanoparticles in $\alpha$ -Fe-based alloys and associated interfacial process

DOI 10.1515/ntrev-2015-0032

Received May 20, 2015; accepted July 31, 2015; previously published online November 6, 2015

**Abstract:** Precipitation of nanoparticles from a supersaturated solid solution is important in understanding and controlling the formation of nanostructure, and as a result, many physical properties of materials, such as conductivity, mechanical, thermoelectric, and magnetic behavior of materials. In each case, the precipitation state, including size, density, chemical composition, spatial distribution, particle morphology, and volume fraction, of nanoparticles can all influence the properties of interest. In an effort to design nano/microstructures in steels, mainly for automotive applications, it is important to be able to describe the time evolution of the precipitation state, including both the nucleation and the growth processes. The present review is thus concerned with the homogenous precipitation of carbo-nitride nanoparticles in  $\alpha$ -ferrite. The interfacial process, the time evolution of both carbon and nitrogen into precipitates, and the effects of supersaturation and spatial distribution are discussed and clarified. The involved mechanisms are discussed from a theoretical point of view; some major results are illustrated from newly developed experimental methods, and their relevance to topics of current interest is examined. At last,

some major outstanding issues have been identified and avenues for further research suggested.

**Keywords:** carbo-nitrides; kinetics; nanoprecipitation; steels; thermodynamics.

## 1 Introduction

The development of modern steels depends on the increased understanding of the role of microalloying elements in the precipitation phenomena in the solid state [1–5]. This topic of major industrial interest has received considerable attention over many years. One of the main reasons for this is that a small addition of microalloying elements may yield significant improvements in mechanical properties [6–11]. Indeed, because of their strong affinity with carbon and nitrogen, microalloying elements such as niobium, vanadium, and titanium form a very fine dispersion of carbides and/or carbo-nitride nanoprecipitates in  $\alpha$ -ferrite. This fine dispersion influences the mechanical properties in a number of ways. The particles interact with matrix dislocations and lead to an increase of global strengthening commonly referred as to “precipitation hardening” (see review in [12]). The fine distribution of precipitates can also inhibit austenite grain coarsening during heating and, under certain circumstances, suppress ferrite recrystallization prior to ferrite-to-austenite transformation in high-strength steels [10, 13]. Besides this, the use of microalloying elements and controlled hot rolling may lead to production of fine ferrite grain through precipitation of fine carbides or carbo-nitrides [14, 15]. In a general manner, the presence of precipitates in  $\alpha$ -Fe matrix can be either beneficial or deleterious for certain manufacturing applications. Indeed, the increase in strength is often accompanied by a reduction in ductility of the material. These properties depend mainly on metallurgical parameters such as nature, density, volume fraction, composition, and morphology of precipitates. Therefore, knowledge and control of the precipitation state is a prime necessity. For this purpose, a double approach

---

\*Corresponding author: Mohamed Gouné, Institute for Condensed Matter and Chemistry of Bordeaux, Centre National de la Recherche Scientifique Unité Propre de Recherche 9048, 87 Avenue du Docteur Schweitzer, 33608 Pessac Cedex, France, e-mail: mm.goune@gmail.com

**Philippe Maugis:** Institut Matériaux Microélectronique Nanosciences de Provence, Aix-Marseille Université et Université de Toulon, Unité Mixte de Recherche Centre National de la Recherche Scientifique 7334, Faculté des Sciences et Techniques, Avenue Escadrille Normandie Niemen, 13397 Marseille Cedex 20, France  
**Frédéric Danoix:** GPM, Université et Institut National de Sciences Appliquées de Rouen, Unité Mixte de Recherche Centre National de la Recherche Scientifique 6634, Normandie Université, Unité de Formation et de Recherche Sciences et Techniques, Avenue de l'Université, BP12, 76801 Saint Etienne du Rouvray, France

based on both experimental and modeling is required. One of the most difficult aspects of any experimental characterization arises from the nanometric size of the precipitates [16–18]. Hence, transmission electron microscopy (TEM) generally has to be undertaken, but further difficulties arise particularly due to the magnetic nature of  $\alpha$ -Fe and the difficulty in measuring the chemistry of nanosized precipitates, especially their carbon and nitrogen contents. The advent and development of new advanced experimental techniques such as TEM and atom probe tomography (APT) is changing this situation. Apart from the experimental aspect, a number of theoretical models have been developed to predict the kinetics, precipitation sequence, and chemistry of the precipitates in microalloyed steels [4, 19–25]. From a kinetic point of view, most of the models are based on the classical theory for diffusive phase transformation and simultaneously treat the nucleation, growth, and coarsening steps from a mean field approach [19, 26, 27]. According to this approach, the nature of the matrix does not modify the analytical form of the laws to be discussed here, only the values of the constants to be used. In the case of pure carbides, the particle size distribution, their number, and volume fraction can be predicted and compared successfully with experimental data [28–30]. Regarding the composition of precipitates, equilibrium conditions are usually assumed for calculations. Nevertheless, the occurrence of nitrogen in solid solution in steels makes the situation more complex. Indeed, one of the main difficulties is accounting for tri-atomic particles having a C/N ratio variable with time [24]. Furthermore, the diffusion rate of both carbon and nitrogen inside the nanoparticles play a more significant role than for pure carbides. In all cases, the interfacial process, including both the interfacial energy between precipitates and  $\alpha$ -Fe and the contact conditions at the precipitates-matrix interface, also plays a key role in the evolution of the precipitation state.

The present review is concerned with the homogenous precipitation in  $\alpha$ -ferrite of carbo-nitride nanoparticles of formula  $M(C_y N_{1-y})$ , M being metallic atoms such as Nb, V, or Ti and C and N being carbon and nitrogen atoms, respectively. “Carbo-nitride” is used as a generic term, and both pure carbides and pure nitrides are considered here to be special cases of carbo-nitrides. However, the precipitation of carbo-nitrides with heterogeneous nitrogen contents induced by nitriding is excluded from the present discussion [31–35].

The interfacial process, the time evolution of both carbon and nitrogen into precipitates, and the effects of supersaturation and spatial distribution are discussed and clarified from a mean field approach. The involved mechanisms are mainly discussed from a theoretical point

of view; some major results are illustrated from developed experimental methods, and their relevance to topics of current interest is examined.

## 2 Homogenous nucleation of carbo-nitrides in $\alpha$ -Fe

The formation of a new phase requires its nucleation in some regions of the system. Homogenous precipitation takes place uniformly in the system considered, contrary to heterogeneous precipitation, which takes place at special sites such as crystal defects. In this chapter, we present the general theory of classical theory. The rate of nucleation is analyzed under quasi-steady-state and non-steady-state conditions, and the influence of the nature of the nucleus-matrix interface is discussed. The effects of strain energy associated to the precipitation of carbo-nitride are not considered in this review.

Nucleation can be defined as the first irreversible formation of a nucleus of the new phase. Fundamentally, it is a stochastic process in which the size of nuclei fluctuates around a critical value. Since its initial formulation in 1926–1927 by Volmer and Weber, and Farkas [36, 37] and its modification in 1935 by Becker and Döring [38], the classical nucleation theory has been a suitable tool to model the nucleation stage in phase transformations. The success of this theory relies on its simplicity and on the few parameters required to predict the nucleation rate, i.e. the number of nuclei of the new phase appearing per unit of time and unit of volume. It allows rationalizing experimental measurements, predicting the consequences of a change of the control parameters such as temperature and supersaturation, and describing the nucleation stage in mesoscopic modeling of phase transformations. In the classical nucleation theory, some of the heterophase fluctuations reach a size large enough so they can continue to grow and lead to the formation of precipitates.

### 2.1 Nucleation rate

The classical nucleation theory is very important in describing the nucleation stage in solid-state phase transformations. From a general point of view, classical nucleation theory assumes that the system reaches a steady state and that the stable nuclei appear at a rate given by the following well-known relation [39, 40]:

$$\frac{dN}{dt} = \beta^* Z N_0 \exp\left(\frac{-\Delta G^*}{k_B T}\right), \quad (1)$$

where  $\beta^*$  is the absorption frequency of a substitutional atom by the critical nucleus,  $Z$  is a dimensionless term often called the Zeldovitch factor, with a magnitude typically close to  $10^3$ ,  $N_0$  is the number of substitutional sites per unit volume in ferrite, and  $\Delta G^*$  is the Gibbs energy barrier. The expression of the nucleation rate initially derived by Volmer and Weber did not contain the Zeldovitch factor and led to an overestimation of the nucleation rate. This Zeldovitch factor was first introduced by Farkas to describe cluster fluctuations around the critical size [37]. Indeed, the nucleation rate would be equal to  $\beta^* N_0 \exp\left(\frac{-\Delta G^*}{k_B T}\right) f$  only if every critical nucleus would continue to grow without going back to smaller sizes. However, the rate theory shows that a nucleus close to the critical size has a non-negligible probability to re-dissolve under thermal fluctuations. The actual nucleation rate is therefore reduced and is given by Eq. (1), where the term  $Z$  corrects for this effect. The quantity  $Z N_0 \exp\left(\frac{-\Delta G^*}{k_B T}\right)$  can also be seen as the number of nuclei that reaches a size large enough to continue their growth. In the case of spherical nuclei, the corresponding radius  $r'$  can be given an analytical approximation [24].

The Zeldovitch factor is a function of the second derivative of the cluster formation free energy at the critical size [41]. It can be shown, from an approach due originally to Zeldovich [42], that  $Z$  is proportional to

$$Z \propto \frac{\sqrt{\sigma^3}}{\Delta G^*}$$

where  $\sigma$  is the interfacial energy between precipitates and ferritic matrix.

The absorption frequency  $\beta^*$  is the frequency at which an additional atom attaches to a critical cluster. It is proportional to the cluster surface area for the reason that the growth-limiting process is the attachment reaction at the interface. As the growth is usually controlled by the long-range diffusion of solute atoms, the absorption frequency is the product of the atom jump frequency with the number of solute atoms contained in a shell of thickness  $a$  ( $a$  being the lattice parameter of  $\alpha$ -Fe) around a spherical cluster:

$$\beta^* = \frac{4\pi r^{*2} D_x^\alpha C_x^\alpha}{a^4},$$

where  $r^*$  is the critical radius,  $D_x^\alpha$  and  $C_x^\alpha$  are the diffusivity and concentration of solute atom in  $\alpha$ -Fe, respectively.

Eq. (1) is often used in a different form that takes into account the so-called incubation time. During incubation, clusters grow from their initial size distribution to a final steady-state distribution. Approximate solutions of the time-dependent nucleation equation discussed by Christian [41] indicate that the time-dependent nucleation rate for a single component system may be approximated by

$$\left. \frac{dN}{dt} \right|_{\text{inc}} \approx \frac{dN}{dt} \exp\left(\frac{-t}{\tau}\right), \quad (2)$$

where  $\left. \frac{dN}{dt} \right|_{\text{inc}}$  is the final quasi-steady-state rate and  $\tau$  is the incubation time. It is interesting to note that, recently, kinetic Monte Carlo simulation has been used to test the classical nucleation theory in the case of homogenous precipitation of niobium carbide (NbC) in  $\alpha$ -Fe [30]. The atomistic approach used is well adapted for studying the very first moments of precipitation including the nucleation step (see an example in Figure 1). Surprisingly, the best fit is provided by a slightly different expression of  $\left. \frac{dN}{dt} \right|_{\text{inc}}$  than Eq. (2):

$$\left. \frac{dN}{dt} \right|_{\text{inc}} \approx \frac{dN}{dt} \left[ 1 - \exp\left(\frac{-t}{\tau}\right) \right]. \quad (3)$$

In all cases, a good estimate for the magnitude of  $\tau$  can be obtained using an argument introduced initially by Russell [40]. Indeed, the incubation time can also be seen as the time to form a significant number of supercritical nuclei. The latter is approximately the time required for clusters to reach size  $r^*$  by absorption and emission of solute atoms at rate  $\beta^*$ . By analogy with the random walk for atomic diffusion along the distance  $\delta=1/Z$  at a jump frequency  $\beta^*$ , the following approximation can be derived:

$$\tau \approx \frac{\delta^2}{2\beta^*}.$$

A specific Taylor expansion of  $\Delta G$  shows that [43]

$$\tau \approx \frac{4}{\pi} \frac{1}{2\beta^* Z^2}. \quad (4)$$

## 2.2 Thermodynamic aspects

In the nucleation regime, the system evolves through localized fluctuations. In a general manner, the Gibbs energy for the formation of nucleus contains two main contributions. The first one is a volume contribution: by

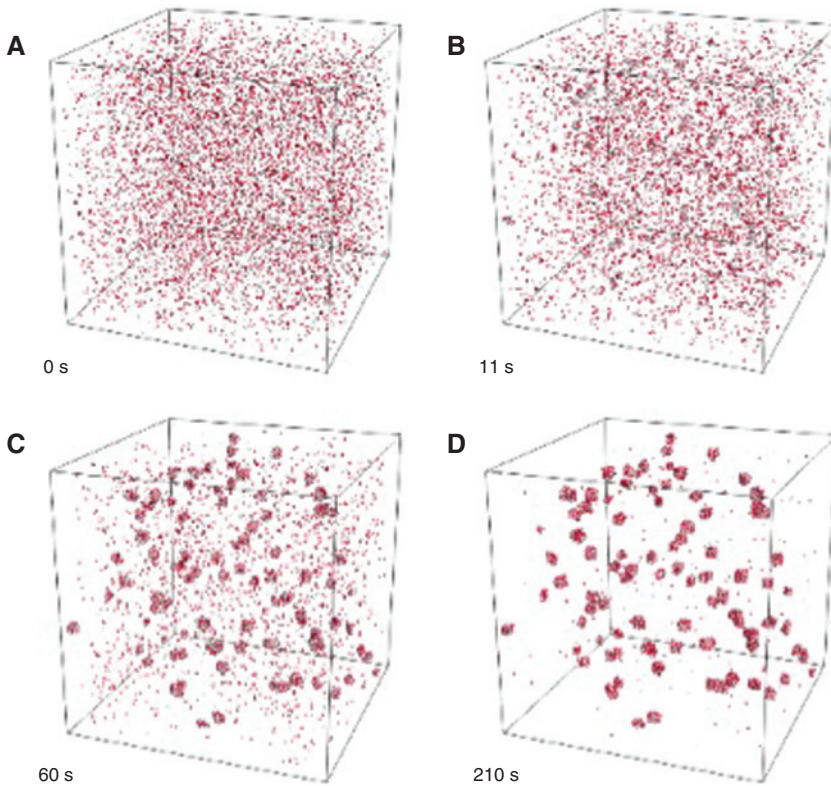


**Figure 1:** An example of Monte Carlo simulation of NbC precipitation in  $\alpha$ -Fe at a given temperature (adapted from [30]). The niobium and carbon atoms are represented in red and gray, respectively, and the corresponding time is given in the bottom left of each snapshot. The density of NbC nuclei can be followed at different times and temperatures.

forming nuclei of the new phase, the system decreases its free energy. The gain is proportional to the nucleation driving force  $\Delta g_v$ . The second one is the surface contribution: the creation of an interface between the matrix and the nuclei of the new phase has a certain cost that depends on the interfacial energy  $\sigma$ . In the case of the formation of a spherical nucleus of carbo-nitride, the following relation is classically considered:

$$\Delta G = \Delta g_v \frac{4}{3} \pi r^3 + \sigma 4 \pi r^2, \quad (5)$$

where  $\Delta g_v$  is the driving energy for nucleation per unit volume (usually called the driving force),  $r$  is the radius of the nucleus, and  $\sigma$  is its interface energy with the matrix. An expression for the driving energy  $\Delta g_v$  is needed for the derivation of the size and composition of the critical nucleus.

In the simplest treatment, the Gibbs energy barrier  $\Delta G^*$  [see Eq. (1)] is obtained as the maximum value of the Gibbs energy as a function of nucleus size (Figure 2). The corresponding size is called the critical size  $r^*$  because the nucleus may be regarded as being in a state of unstable equilibrium with the surrounding parent phase. From a

mathematical point of view, this results in the following relations:

$$\left\{ \begin{array}{l} \frac{\partial(\Delta G)}{\partial r} \Big|_{r=r^*} = 0 \\ r^* = \frac{-2\sigma}{\Delta g_v} \\ \Delta G^* = \frac{16\pi}{3} \frac{\sigma^3}{\Delta g_v^2} \end{array} \right. \quad (6)$$

The determination of both the driving force and the interface energy is crucial for calculating both the Gibbs energy barrier and, as a result, the nucleation rate [see Eq. (1)].

### 2.2.1 Driving force for nucleation

Let us imagine the formation of a  $\beta$  phase of formula  $M(C_y N_{1-y})$  from a solid solution  $\alpha$ -Fe. The driving force for nucleation can be regarded as the quantity of the free energy transferred to  $dn$  molecules of  $M(C_y N_{1-y})$  from the supersaturated solid solution to the precipitate, which is in equilibrium with the  $\alpha$ -Fe solid solution. In the simple

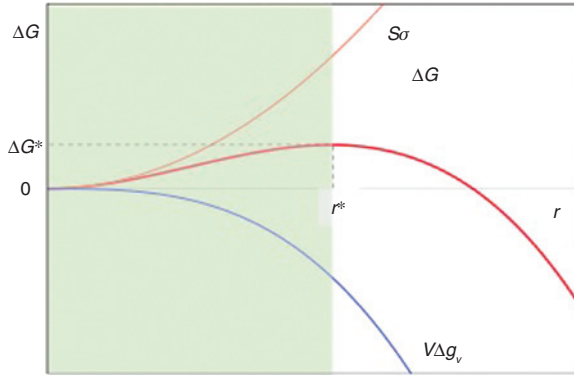


**Figure 2:** Schematic evolution of the Gibbs energy during the formation of a spherical nucleus as a function of the radius of the particle. Both the surface and volume contributions are shown (adapted from [44]).

case of a binary compound of formula AB, the driving force for nucleation  $\Delta g_v$  is schematically represented in Figure 3.

By generalizing the simple case of a binary compound to a ternary compound of formula  $M(C_yN_{1-y})$ , one can write

$$V_m \Delta g_v = [x_M^\beta \mu_M^\beta(x_M^\beta) + x_C^\beta \mu_C^\beta(x_C^\beta) + x_N^\beta \mu_N^\beta(x_N^\beta)] - [x_M^\alpha \mu_M^\alpha(x_M^\alpha) + x_C^\alpha \mu_C^\alpha(x_C^\alpha) + x_N^\alpha \mu_N^\alpha(x_N^\alpha)], \quad (7)$$

where  $\mu$  is the chemical potential. The equilibrium between the  $\beta$  phase and  $\alpha$ -Fe imposes the classical following relation:

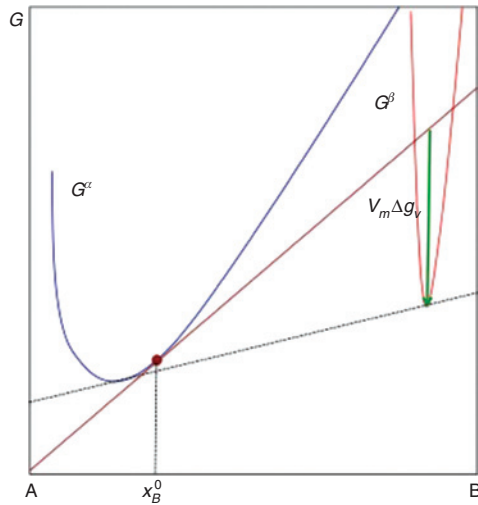


**Figure 3:** Schematic representation of the driving force for nucleation  $\Delta g_v$  from the Gibbs energy diagram in a model A–B binary alloys. In the simplest approach, the product  $V_m \Delta g_v$ ,  $V_m$  being the molar volume of the precipitate  $\beta$ , is determined from the common tangent (in dashed line) to  $G^\alpha$  and  $G^\beta$  and the tangent to  $G^\alpha$  passing through the nominal composition  $x_b^0$  of the given alloy [45].

$$\mu_i^\beta(x_i^\beta) = \mu_i^\alpha(x_i^{\alpha,e}),$$

where  $x_i^{\alpha,e}$  is the equilibrium composition of the  $i$  element in  $\alpha$ -Fe.

Therefore, relation (7) becomes

$$V_m \Delta g_v = [x_M^\beta \mu_M^\alpha(x_M^{\alpha,e}) + x_C^\beta \mu_C^\alpha(x_C^{\alpha,e}) + x_N^\beta \mu_N^\alpha(x_N^{\alpha,e})] - [x_M^\beta \mu_M^\alpha(x_M^0) + x_C^\beta \mu_C^\alpha(x_C^0) + x_N^\beta \mu_N^\alpha(x_N^0)].$$

By taking into account the stoichiometry of precipitates, we obtain the following equation:

$$V_m \Delta g_v = \left[ \frac{1}{2} \mu_M^\alpha(x_M^{\alpha,e}) + \frac{1}{2} y \mu_C^\alpha(x_C^{\alpha,e}) + \frac{1}{2} (1-y) \mu_N^\alpha(x_N^{\alpha,e}) \right] - \left[ \frac{1}{2} \mu_M^\alpha(x_M^0) + \frac{1}{2} y \mu_C^\alpha(x_C^0) + \frac{1}{2} (1-y) \mu_N^\alpha(x_N^0) \right].$$

The chemical potentials are thus developed as a function of the molar fractions according to the ideal solid solution assumption, and the concentrations in solid solution  $x_i^{ss}$  are also introduced. This leads to the following expression [22, 24, 46]:

$$\Delta g_v = -\frac{RT}{2V_m} \left[ \ln \frac{x_M^{ss}}{x_M^{\alpha,e}} + y \ln \frac{x_C^{ss}}{x_C^{\alpha,e}} + (1-y) \ln \frac{x_N^{ss}}{x_N^{\alpha,e}} \right]. \quad (8)$$

## 2.2.2 Composition of the critical nucleus

Relation (8) clearly shows that, contrary to the case of pure carbide or pure nitride, the driving force for nucleation of a carbo-nitride depends on its stoichiometry parameter  $y$ , which gives the carbon and nitrogen contents in the precipitate. There is no objective reason to consider *a priori*  $y$  as a constant during nucleation and growth of the precipitate.

Eq. (8) uses the equilibrium composition of each element  $i$  in  $\alpha$ -Fe  $x_i^{\alpha,e}$ . Strictly speaking, their determination requires a complex thermodynamic calculation. However, it is possible to overcome this difficulty, as shown in [24, 47]. Indeed, the equilibrium between the ferrite matrix and the carbo-nitride  $M(C_yN_{1-y})$  can be described by the following mass action law under the assumption of ideal solution:

$$RT [\ln x_M^{\alpha,e} + y \ln x_C^{\alpha,e} + (1-y) \ln x_N^{\alpha,e}] = \Delta G_{M(C_yN_{1-y})}^0, \quad (9)$$

where  $\Delta G_{M(C_yN_{1-y})}^0$  is the Gibbs energy of formation of the carbo-nitride. The carbide MC and the nitride MN are often both of face-centered cubic NaCl-type crystal structure with very similar molar volumes. We thus consider

the carbo-nitride as an ideal mix of MC and MN, and following Hillert and Staffansson [48], we can write

$$\Delta G_{M(C,N_{1-y})}^0 = y\Delta G_{MC}^0 + (1-y)\Delta G_{MN}^0 + RT[y\ln y + (1-y)\ln(1-y)], \quad (10)$$

where  $\Delta G_{MC}^0$  and  $\Delta G_{MN}^0$  are the Gibbs energy of formation of MC and MN, respectively. Eq. (10) gives a thermodynamic representation of a complex carbo-nitride from the thermodynamic of corresponding pure carbide and nitride. However, Eq. (10) does not account for a possible interaction between MC and MN. In other words, the excess molar free energy of mixing of MC and MN is neglected.

The thermodynamic functions  $\Delta G_{MC}^0$  and  $\Delta G_{MN}^0$  are related to the solubility products for the individual MC and MN compounds in equilibrium with the matrix by the following classical relations:

$$\begin{cases} \ln(x_M^{\alpha,e} \cdot x_C^{\alpha,e}) = \frac{\Delta G_{MC}^0}{RT} \\ \ln(x_M^{\alpha,e} \cdot x_N^{\alpha,e}) = \frac{\Delta G_{MN}^0}{RT} \end{cases} \quad (11)$$

By substituting Eq. (10) into Eq. (9), it is easy to show according to [49, 50] that

$$\begin{cases} yK_{MC} = x_M^{\alpha,e} \cdot x_C^{\alpha,e} \\ (1-y)K_{MN} = x_M^{\alpha,e} \cdot x_N^{\alpha,e} \end{cases} \quad (12)$$

where  $K_{MC}$  and  $K_{MN}$  are the product solubility of carbide MC and nitride MN, respectively.

Using Eq. (12), the unknown equilibrium composition in solid solution  $x_i^{\alpha,e}$  can be replaced by the solubility products of carbide  $K_{MC}$  and of nitride  $K_{MN}$  into Eq. (8):

$$\Delta g_v = -\frac{RT}{2V_m} \ln \left[ \frac{(x_M^{ss})^y (x_C^{ss})^y (x_N^{ss})^{1-y}}{(yK_{MC})^y [(1-y)K_{MN}]^{1-y}} \right]. \quad (13)$$

It is thus stated that the nuclei that appear in the matrix are those that produce the maximum variation of Gibbs energy during their formation. Accordingly, the composition of the critical nucleus is defined as the value of  $y$  that minimizes the driving force for nucleation in Eq. (13). The expression is found to be

$$y_{\text{nucl}} = \left[ 1 + \frac{x_N^{ss} K_{MC}}{x_C^{ss} K_{MN}} \right]^{-1}. \quad (14)$$

This equation shows that the composition  $y_{\text{nucl}}$  of the critical nucleus does not depend on the metallic atoms

concentration  $M$  in the solid solution and depends exclusively on the temperature, *via* the ratio of the solubility products, and on the C and N composition of the solid solution.

If carbon and nitrogen in a solid solution are of equal orders of magnitude, the nucleus will be very rich in nitrogen because the nitride of a given material is much more stable thermodynamically than the corresponding carbide, as shown by the temperature evolution of solubility product of some nitrides and carbides given in Figure 4 [2, 51].

Obviously, the composition of both C and N in nuclei is expected to evolve with time at a given temperature because the compositions in solid solution decrease during the precipitation process. Accessing

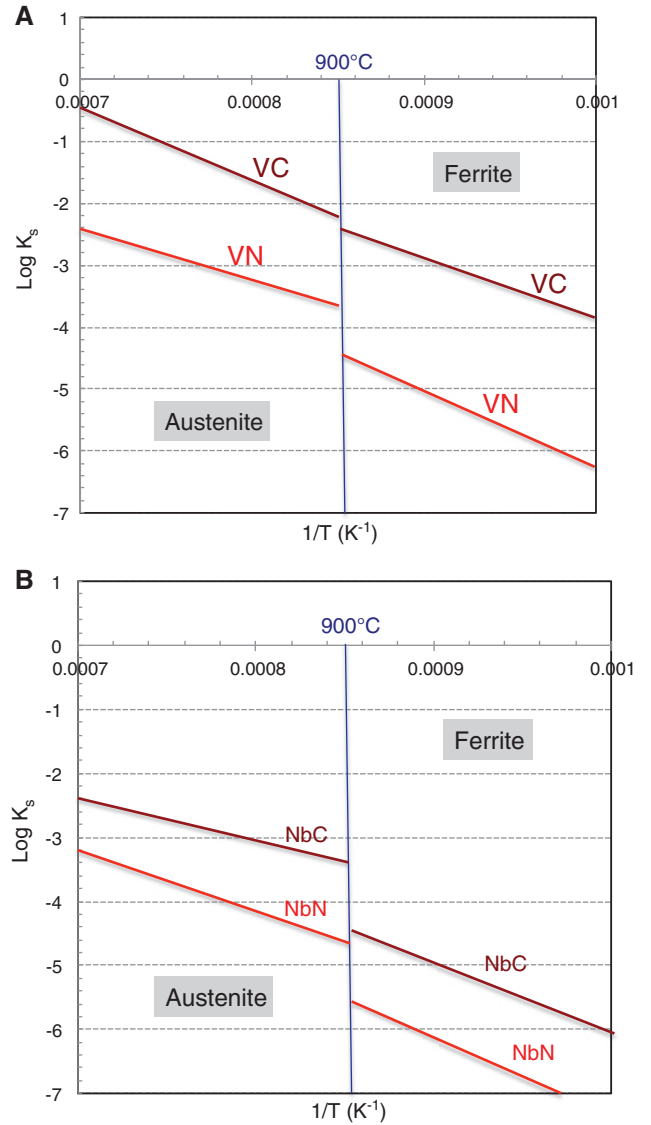


Figure 4: Solubility data. (A) VC and VN, (B) NbC and NbN [51].

composition information of such nanoprecipitates can be achieved through techniques combining analytical capabilities with sub-nanometer-scale spatial resolutions. TEM remains the most widely used high-resolution technique (in imaging and analytical modes). One of the most challenging problems that has to be addressed for TEM/STEM chemical characterization of carbo-nitrides is specimen preparation. Indeed, specimens have to be electron transparent, i.e. must have a thickness smaller than 100 nm. Even for thin specimens, the thickness of the foil is significantly larger than the particle diameter. Conducting an analytical investigation of such embedded precipitates will lead inevitably to a mixed matrix-precipitates analysis. Only when the elements of interest in the precipitate are completely depleted in the matrix can a quantitative chemical analysis of the particle be achieved. An alternative specimen preparation has been developed, namely extraction replicas. It consists of dissolving the surrounding matrix after deposition of an electron transparent film. Most widely used films are amorphous carbon, but for evident reasons, the presence of carbon in the film has to be ruled out. Therefore, alternative aluminum oxide-based films are preferred. Using extraction replicas based on either sub-stoichiometric radiofrequency (RF)-sputtered amorphous  $\text{Al}_x\text{O}_y$  ( $x \approx y \approx 1$ ) films or DC-sputtered bilayer  $\text{Al}_2\text{O}_3/\text{Al}$  films, Scott and Drillet [52] have shown that as long as no residual C or N signal was originating from the oxide films, C sensitivity as low as 0.04 wt% can be achieved [52]. Using this approach, quantitative determination of absolute C and N content in nanoprecipitates could be obtained [17, 51, 53]. In particular, regarding the evolution of carbo-nitride composition, as shown in Figure 5, Scott has demonstrated a clear evolution of the N/(C+N) ratio as a function of carbo-nitride size. As the precipitate size increases with ageing time, this evolution can also be regarded as an evolution of their composition with time.

### 2.2.3 Particular sequence of precipitation

A particular nucleation mechanism has recently been shown in model FeNb(CN) alloys. Indeed, a combined field ion microscopy (FIM), APT, and high-resolution electron microscopy (HRTEM) investigation of the early stages of precipitation has demonstrated the existence of Guinier Preston (GP) zones. GP zones, which are well known and documented in the precipitation sequence of aluminum-based alloys [55], are particular nuclei of a second phase that adopt the same structure as the parent matrix. In most cases, they adopt a particular platelet shape, with one or several atomic planes in thickness. Such platelets have been observed not only in model FeNb(CN) alloys, as shown in Figure 6, but also in nitrated FeTi [57] and FeCr [58] alloys and in industrial steels [59, 60], leading to high strength increase.

## 2.3 Interfacial energy

The interface energy  $\sigma$  between particles and  $\alpha$ -Fe matrix plays a key role on both nucleation and growth steps. It is clear through Eqs. (1) and (6) that a small change in  $\sigma$  can lead to a dramatic change in the calculated nucleation rate. As a consequence, the knowledge of  $\sigma$  is a prime necessity for studying the precipitation of carbo-nitrides in ferrite, even if its experimental determination is a tedious process [61] and a wide range of values has been reported [22, 23, 26, 30, 62]. Also, it is important to recognize that the most common approach is to consider the interface energy  $\sigma$  as a fitting parameter that is, for the sake of simplicity, often considered as a constant value [23, 26, 28, 30, 62]. Obviously, there are some clear limitations to this approach as discussed below.

In a general manner, and from a theoretical point of view, the interfacial energy can be calculated from the

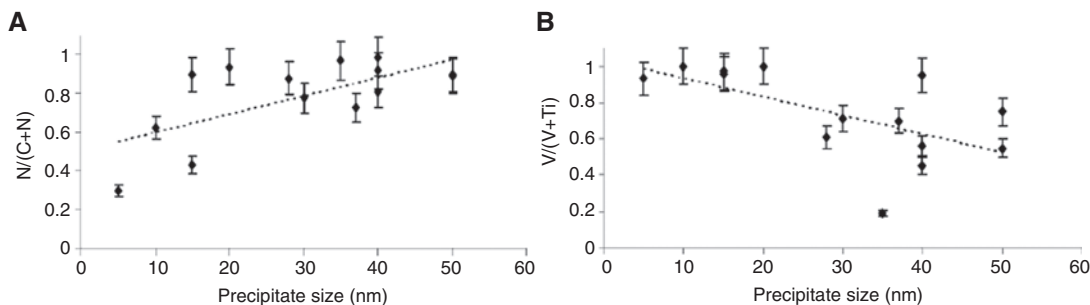


**Figure 5:** (A) PEELS measurements of precipitate nitrogen to carbon atomic ratios in proeutectoid ferrite of a ferrite-pearlitic microalloyed vanadium steel Fe-0.38C-0.107V-0.010Ti-0.026Al-0.015 N. The steel had been austenitized at 1250°C for 1 min, deformed above 1000°C, and air cooled to 20°C at 1000°C/h. (B) The corresponding vanadium-to-titanium atomic ratios as measured by EDX [54].



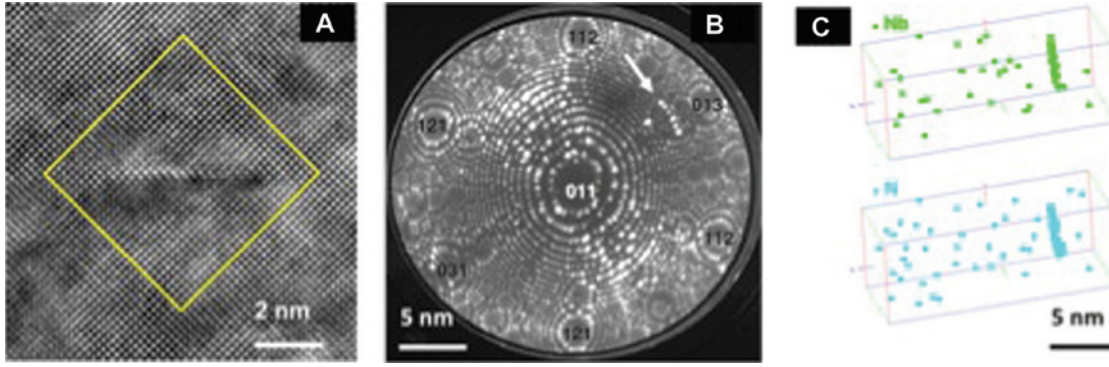


**Figure 6:** Atomic-scale evidence of GP zones in FeNbCN model steel. (A) HRTEM, (B) FIM, and (C) APT [56].

difference in cohesive energies between the interfacial region and the bulk:

$$\sigma = E_{\alpha\text{-Fe}/\text{M}(\text{C},\text{N})} - \frac{1}{2}(E_{\alpha\text{-Fe}/\alpha\text{-Fe}} - E_{\text{M}(\text{C},\text{N})/\text{M}(\text{C},\text{N})}), \quad (15)$$

where  $E_{\alpha\text{-Fe}/\text{M}(\text{C},\text{N})}$  is the sum of bonding energies across the  $\alpha$ -Fe/M(C,N) carbo-nitride interface and  $E_{\alpha\text{-Fe}/\alpha\text{-Fe}}$  and  $E_{\text{M}(\text{C},\text{N})/\text{M}(\text{C},\text{N})}$  are the sum of the bonding energies across the planes parallel to the interface in the ferrite matrix and M(C,N) carbo-nitride, respectively [63]. A value of interface energy of 493 mJ/m<sup>2</sup> was calculated for coherent  $\alpha$ -Fe/TiC interface [63]. This value can be compared with the value of 1.22 J/m<sup>2</sup> for coherent  $\alpha$ -Fe/NbC interface adjusted from Monte Carlo calculations [30] and with the value of 0.78 J/m<sup>2</sup> for  $\alpha$ -Fe/Nb(C<sub>y</sub>N<sub>1-y</sub>) adjusted from the time evolution of the measured chemical composition of carbo-nitrides [25]. These values of interfacial energy are not directly calculated but fitted using a mean field model for precipitation. Therefore, they are source of possible error.

The interface energy  $\sigma$  given in Eq. (15) includes a contribution from both the chemical bonding energy and the structural strain energy [63, 64].

This would suggest that the interfacial energy depends on the degree of interface coherency. Accordingly, it is often proposed to express the interfacial energy as [65]

$$\sigma = \sigma_0 + C_1(\delta - \varepsilon), \quad (16)$$

where  $\sigma_0$  is the interfacial energy of a coherent interface,  $C_1$  is a coefficient related to dislocation density,  $\delta$  is the misfit between the two lattices, and  $\varepsilon$  is the strain at the interface ( $\varepsilon=0$  for an incoherent interface and  $\varepsilon=\delta$  for a coherent interface). Therefore,  $\sigma$  varies from low values for coherent interfaces to high values for incoherent interfaces, and thus, nuclei with coherent interfaces precipitate preferentially [66].

Most of the carbides and carbo-nitrides [TiC, NbC, V(C,N), etc.] exhibit a face-centered cubic crystal structure

form with the NaCl structure and have a Baker-Nutting orientation relationship with the ferrite matrix [11, 30, 67, 68].

A schematic illustration of the atomic configuration at the interface between bcc-Fe and MC carbide having the Baker-Nutting orientation relationship ( $(100)_{\alpha} // (100)_{\text{M}(\text{C},\text{N})}$   $[010]_{\alpha} // [011]_{\text{M}(\text{C},\text{N})}$ ) is given in Figure 7.

The lattice parameters of most carbides and nitrides are between 0.4 and 0.48 nm [69, 70]. The lattice misfit between ferrite and carbide or carbo-nitride, defined as  $\delta = \frac{a_{\text{M}(\text{C},\text{N})} - \sqrt{2}a_{\alpha\text{-Fe}}}{a_{\text{M}(\text{C},\text{N})}}$ , is thus between 3% and 15% (see Figure 8).

As a consequence, a contraction of the M(C,N) lattice is necessary to maintain the coherency at the interface with the ferrite matrix. This leads to two main remarks. First, the elastic strain energy associated to the precipitation of coherent M(C,N) in  $\alpha$ -Fe can be significant and

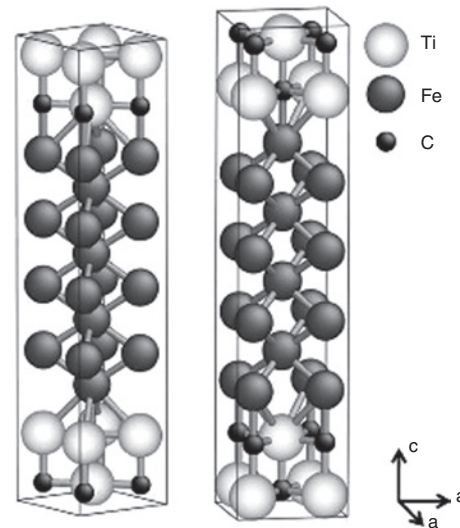


**Figure 7:** Schematic illustration of atomic arrangement of a coherent  $\alpha$ -Fe/TiC interface with the Baker-Nutting orientation relationship.

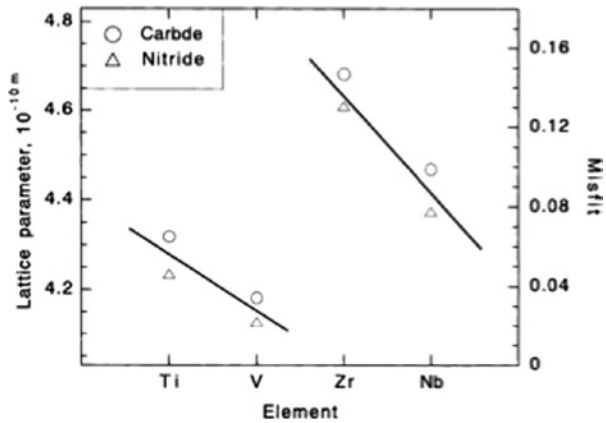


Figure 8: Lattice misfit of carbides and nitrides with  $\alpha$ -Fe matrix [67].

should not be considered as negligible with respect to the driving force for nucleation [71, 72]. Second, for this large atomic misfit, it would be energetically favorable to replace the coherent interface with a semi-coherent interface and even an incoherent interface. This operates through dislocations that are introduced in the interface to accommodate the misfit between the two phases. Therefore, the result is a coherency loss, and the interfacial energy is expected to evolve with time during the precipitation process. In general,  $\sigma$  ranges between 200 and 500 mJ/m<sup>2</sup> during nucleation (for a semi-coherent interface) and may reach up to 1 J/m<sup>2</sup> during growth and coarsening (for an incoherent interface). This aspect is often neglected in many models of precipitation of carbo-nitride in ferrite [23, 24, 26, 62]. Furthermore, as noted by [30, 67], the chemical interface energy between Baker-Nutting-oriented ferrite and carbo-nitrides is likely to be highly anisotropic, and as a consequence, the assumption of spherical nuclei is certainly questionable in many cases.

## 3 Growth

### 3.1 Laws for growth: case of the mono-atomic precipitate

In this section, we deal with the laws of growth of precipitates. The nature of the matrix does not modify the analytical form of the laws to be discussed here, only the values of the constants to be used. Let us then consider one precipitate observed at the end of its homogeneous nucleation process. It is embedded in a supersaturated  $\alpha$ -Fe matrix, the composition of which is supposed to

be uniform at this stage. As a result, the precipitate will spontaneously grow by incorporating solute atoms. This process involves three physical phenomena that will be analyzed in sequence:

1. local equilibrium at the precipitate-matrix interface,
2. solute transport toward the interface,
3. precipitate-matrix interface motion.

For the sake of simplicity, the inherent simplifications in the mean field modeling are discussed from the simple case of mono-atomic precipitates (for example, the case of precipitation of copper in binary Fe-Cu). Most of the assumptions remain valid for the growth of bi-atomic MC or MN or tri-atomic M(C,N). This is justified by realizing that the kinetics of growth of a carbide or carbo-nitride are limited by the diffusion of the slow substitutional atom (M), with the interstitial atoms (C and N) being very fast diffusers. In the following paragraphs, we will introduce the necessary refinements when extending the growth laws to the bi-atomic MC and to M(C,N) precipitates.

#### 3.1.1 Hypotheses

Let us consider a precipitate of composition  $x_i^\beta$  growing in a matrix of composition  $x_i^{ss}$ . The usual hypotheses for an elementary treatment are the following:

1. the precipitate is spherical,
2. local equilibrium stands at the precipitate-matrix interface,
3. the precipitate growth is limited by solute diffusion in the matrix.

In a binary system, local equilibrium at the interface simply states that the precipitate and matrix compositions in the immediate vicinity of the interface keep their values prescribed by the thermodynamic equilibrium at the given temperature. This constrained local equilibrium creates a composition gradient in the matrix, which is the driving force for solute diffusion toward the precipitate.

#### 3.1.2 Various approximations for parabolic growth

The kinetic law for growth  $r(t)$  is the solution of both conditions: (i) mass conservation at the interface and (ii) solution of the diffusion equation in the matrix. Assuming that the diffusion coefficient in the matrix is a constant  $D$ , various approximations are possible for the diffusion problem, depending on the expression of the solute diffusion flux at the interface. Starting from an infinitely small

precipitate ( $r=0$  at  $t=0$ ), all solutions have the form of a parabolic growth

$$r^2(t) = \lambda^2 Dt, \quad (17)$$

where  $\lambda^2$  is a constant (for more details, see [73]) and is a function of the supersaturation ratio  $k$  defined as

$$k = 2 \frac{x_i^{ss} - x_i^{\alpha/\beta}}{x_i^\beta - x_i^{\alpha/\beta}}, \quad (18)$$

where  $x_i^{\alpha/\beta}$  is the concentration of  $i$  at the interface on the matrix side.

Three approximations, valid for small supersaturation values, are in decreasing order of precision: (1) the exact solution, (2) the stationary interface approximation, and (3) the invariant field approximation, for which  $\lambda_2 = k$ . The functions  $\lambda_2(k)$  are drawn in Figure 9.

As can be seen in Figure 9, the three approximations meet when  $k$  tends to zero. In usual situations of microalloying, the solute fractions in solid solution are  $<0.1$  at%. As a consequence, the supersaturation ratio is usually  $<10^{-3}$ . Under this condition, the three approximations are within a relative difference of  $<1\%$ . They can be considered practically equivalent. Thus, the invariant field approximation can safely be adopted for its simplicity. Under its differential form, it is known as the Zener equation [74]. It is expressed, assuming that both phases have the same molar volume, as

$$\frac{dr}{dt} = \frac{D_i^\alpha}{r} \frac{x_i^{ss} - x_i^{\alpha/\beta}}{x_i^\beta - x_i^{\alpha/\beta}}, \quad (19)$$

where  $r$  is the radius of particle and  $D_i^\alpha$  is the diffusion coefficient of element  $i$  in the ferritic matrix. This equation

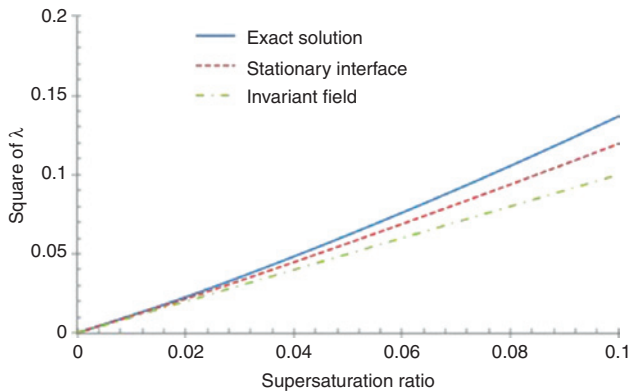


**Figure 9:** Laws for growth in an infinite medium. Comparison of the various approximations:  $\lambda^2$  parameter as a function of the supersaturation ratio  $k$ .

is also valid in the case of precipitate dissolution. It can be used for non-isothermal situations where both  $x_i^{ss}$  and  $D_i^\alpha$  vary with time and temperature. In the general case, Eq. (19) has to be integrated numerically, starting from any initial situation ( $r=r_0$  at  $t=t_0$ ).

### 3.1.3 The Gibbs-Thomson effect

Direct use of the invariant field solution is, however, scarcely possible. The first reason is that the Gibbs-Thomson effect has to be taken into account for nanometer-scale precipitates. The latter was first observed for small liquid particles in equilibrium with gas by Thomson [75]. Then, Gibbs formulated a relation for the concentration evolution around small curved particles [76]. In fact, the interface curvature introduces a deviation in the matrix local concentration as a function of the precipitate radius:

$$x_i^{\alpha/\beta}(r) = x_i^{\alpha/\beta}(\infty) \exp\left(\frac{2\sigma V_p}{r RT}\right), \quad (20)$$

where  $x_i^{\alpha/\beta}(\infty)$  is the equilibrium value given by the phase diagram, i.e. for a precipitate of infinite radius,  $\sigma$  is the interfacial energy,  $V_p$  is the molar volume of the precipitate, and  $R$  is the gas constant. In this case, the invariant field solution is no longer valid. However, the Zener equation [Eq. (19)] can still be used and integrated numerically, provided the  $x_i^{\alpha/\beta}(r)$  expression given in Eq. (20) is used.

### 3.1.4 Effect of solute exhaustion

Precipitation of the solute atoms naturally leads to a decrease of the solute content in the matrix: the hypothesis that  $x_i^{ss}$  remains constant is true only for short reaction times. In general, solute depletion of the matrix has to be taken into account to get a proper kinetic law. Various expressions for the mass balance can be written, depending on the geometry of the problem, and yield an expression of  $x_i^{ss}$  as a function of  $r$  to be inserted in the Zener equation [Eq. (19)]. That insertion ensures that for a long isothermal annealing,  $x_i^{ss}$  will tend properly to its equilibrium value given by the phase diagram and that the particle radius will tend to its asymptotic value.

### 3.1.5 Effect of spatial distribution

As a result of the nucleation stage, or as a result of the fabrication process, the spatial distribution of the particles

will rarely be uniform. On the contrary, some of the particles will be clustered, whereas some regions will look particle-free, at least in a two-dimensional (2D) section. During growth, when the diffusion length scale reaches the average distance between the particles, the growth kinetics of a given particle will be influenced by its neighboring particles (effect called soft impingement). Knowing this, the question is whether the time evolution of the average radius of the particles is accurately predictable.

A three-dimensional (3D) model has been used and is illustrated in Figure 10A. Precipitates of the same radius  $r_0$  were randomly distributed over space, and the growth of each particle has been calculated through a 3D finite volume scheme [30]. We observe that clustered particles, having to share the solute atoms with one another, grow slower than the isolated ones. However, it appears that the average radius  $\langle r \rangle$  of the distribution obeys a kinetics that is exactly that of a single representative particle of initial size  $r_0$  (Figure 10B). In other words, the mean field approximation is fully justified here.

### 3.1.6 Effect of size distribution

In most situations, the knowledge of the average radius of precipitates together with their volume number is enough information for practical use, in particular, for the evaluation of the mechanical properties of the alloy. In some cases, however, the whole size distribution can be of importance. Kampmann and Wagner [19] provided two numerical approaches in this prospect: (i) in the Langerian approach, the particles are distributed in classes of age, whereas (ii) in the Eulerian approach, the particles are distributed along existing classes of size. Both

approaches yield the same results in terms of mean radius and volume number [77]. Furthermore, in cases where the size distribution is monomodal, the mean field approach based on the average precipitate radius has proven to be an excellent approximation, together with a very high computing efficiency.

## 3.2 Bi-atomic precipitate

The growth of a bi-atomic precipitate such as NbC or NbN precipitate can be treated similarly to the case of a mono-atomic precipitate: as diffusion of the metallic atoms will be rate limiting, allowing for the use of a variant of the Zener equation. However, coupling of the local equilibrium condition with the local flux compatibility at the interface has to be taken into account to evaluate the interfacial concentration.

During the growth of a carbide MC, for example (the treatment would be the same for a pure nitride MN), a gradient in M concentration builds up around the precipitate. As carbon atoms diffuse very much faster, the concentration profile of carbon remains almost flat, assuming no carbon-metal interaction. The Zener equation is then written as, with obvious notations,

$$\frac{dr}{dt} = \frac{D_M^\alpha}{r} \frac{x_M^{ss} - x_M^{\alpha/\beta}}{V_{Fe}/V_{MC} - x_M^{\alpha/\beta}}. \quad (22)$$

In this equation, the use of atomic fractions makes the ratios  $V_{Fe}/V_{MC}$  appear, where  $V_{MC}$  is the volume of 1 mol of MC. In the ternary Fe-M-C phase diagram, the local equilibrium at the precipitate-matrix interface takes the form of a solubility product, modified by the Gibbs-Thomson effect:

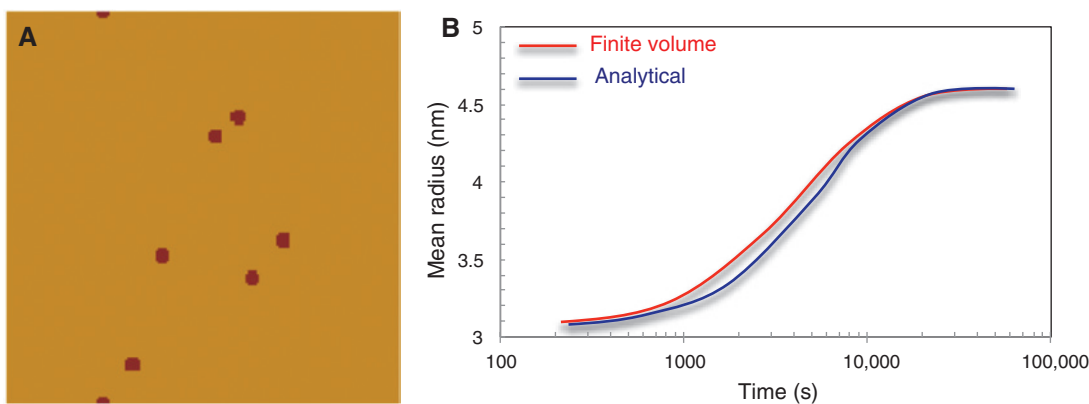


**Figure 10:** Effect of the spatial distribution of nuclei on the growth kinetics. (A) Initial state of the finite volume calculations (2D section, precipitates in red). (B) Time evolution of the mean radius compared to the analytical model [Eq. (19)] [30].

$$X_M^{\alpha/\beta} X_C^{\alpha/\beta} = K_{MC} \exp\left(\frac{2\sigma V_{MC}}{r RT}\right), \quad (23)$$

where  $K_{MC}$  is the solubility product for MC in the matrix. This equation is an approximation that holds only in the case of diluted solid solution and stoichiometric precipitates. For the general case of multicomponent precipitates and non-dilute solid solution, the reader can refer to [78]. Eq. (23) is not enough to determine the interfacial M concentration in the matrix  $X_M^{\alpha/\beta}$ , and a compatibility equation has to be used. In the general case, the compatibility condition originates from the equality of the growth rates of Eq. (22), whichever solute element of reference is used (C or M). The simplest approach, valid as long as the matrix is dilute compared to the precipitate composition, is to write the flux compatibility condition: the incoming fluxes of C and M have to be equal at the interface for the stoichiometry of MC to be respected. In the invariant field approximation, this is written as

$$D_C^\alpha (X_C^{\alpha/\beta} - X_C^{ss}) = D_M^\alpha (X_M^{\alpha/\beta} - X_M^{\alpha/\beta}), \quad (24)$$

Eq. (24) defines an almost vertical straight line in the  $(x_C, x_M)$  isotherm graph (Figure 11). Graphically, the solution of the set of Eqs. (23) and (24) is the intersection between the equilibrium isotherm and the flux compatibility line. During an isothermal precipitation treatment, the matrix composition decreases along the stoichiometry line, and consequently, the M interfacial composition  $X_M^{\alpha/\beta}$  increases from an initial value to its equilibrium value.

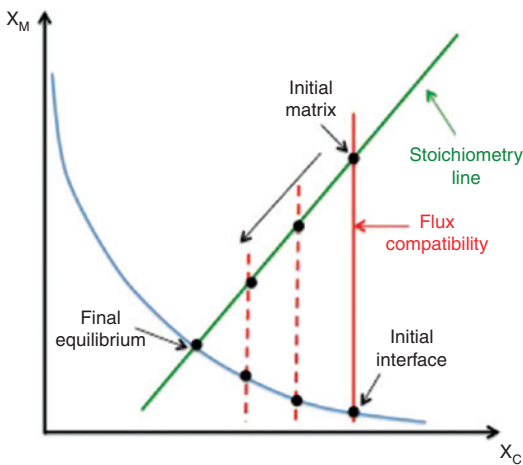


**Figure 11:** Time evolution of the matrix and interfacial compositions during an isothermal heat treatment. For clarity, the Gibbs-Thomson effect has been neglected here.

### 3.3 Growth of carbo-nitride M(C,N): the core-shell model

A major difference with the previous case is that a carbo-nitride  $M(C_y N_{1-y})$  allows for a wide range of composition on the interstitial sub-lattice: in fact, possible carbo-nitrides of general formula  $M(C_y N_{1-y})$  range from MC ( $y=1$ ) to MN ( $y=0$ ), and the composition of a given particle will gradually change with time during its growth. Consequently, the composition distribution has to be taken into account together with the size distribution of the particles. The mathematical treatment developed in [24] is summarized in the following.

The kinetic equation for growth is analogous to that for MC and is written as

$$\frac{dr}{dt} = \frac{D_M^\alpha}{r} \frac{X_M^{ss} - X_M^{\alpha/\beta}}{V_{Fe} / V_{M(C_y N_{1-y})} - X_M^{\alpha/\beta}}, \quad (25)$$

where  $V_{M(C_y N_{1-y})}$  is the volume of 1 mol of  $M(C_y N_{1-y})$ . Growth occurs by accretion of successive shells of variable composition  $y$ . The calculation of the shell composition is done together with the calculation of the matrix composition in the vicinity of the interface by the simultaneous resolution of the local equilibrium and the flux compatibility conditions, Maugis and Gouné [24] showed that a very good approximations is given by

$$\frac{1-y_g}{y_g} = \frac{X_M^{ss} K_{MC}}{X_C^{ss} K_{MN}} \text{ and } X_M^{\alpha/\beta} = \left( \frac{X_C^{ss}}{K_{MC}} + \frac{X_N^{ss}}{K_{MN}} \right)^{-1}. \quad (26)$$

It appears that, for each time interval, the composition of the shell  $y_g$  during growth is the same as that of the critical nucleus [see Eq. (14)] and is only driven by the composition of carbon and nitrogen in the solid solution, irrespective of the diffusion coefficients of M, C, and N.

The model allows for describing the evolution of the precipitation state of  $M(C_y N_{1-y})$  particles in a ferritic matrix, as shown in Figure 12.

In the core-shell model used here, carbon-nitrogen interdiffusion inside the particle is supposed to be very slow compared to the diffusion in the matrix. The alternative hypothesis of infinitely fast intraparticle diffusion could have been used, which would have led to slightly different results: in particular, under this second hypothesis, the precipitate equilibrium composition would be reached at the end of the growth regime, which is contrary to our experimental measurements (see Figure 12).

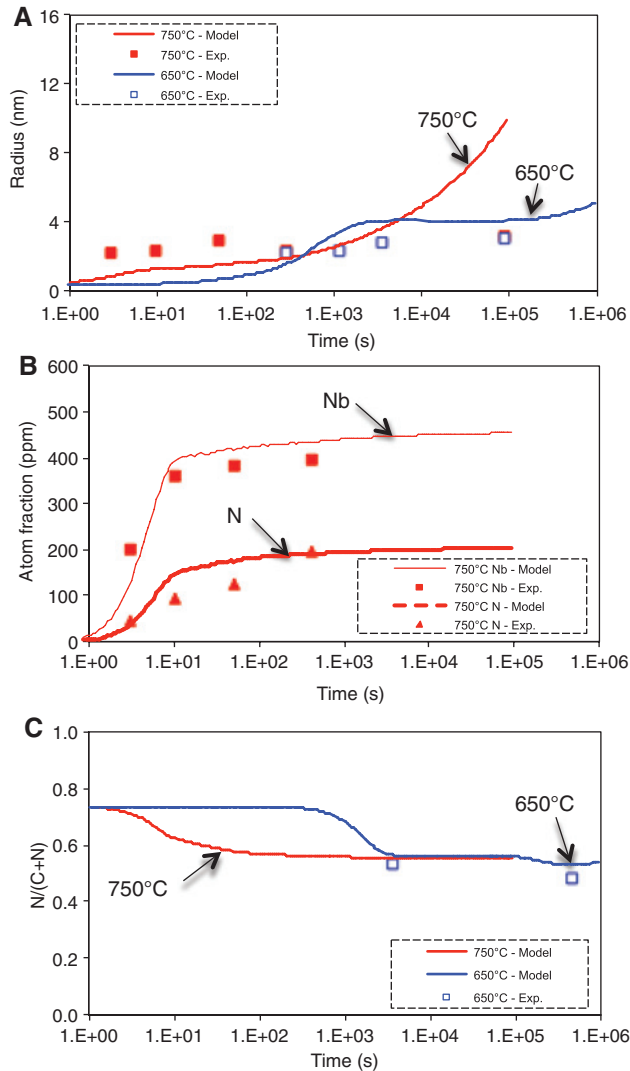


**Figure 12:** Time evolution of the precipitation state in a Fe-Nb-C-N alloy aged at 750°C and 650°C. (A) Comparison between the calculated and the measured mean radius at both 650°C and 750°C. (B) Comparison between the calculated and measured nitrogen and niobium precipitate elements at 750°C. (C) Calculated mean composition of precipitates at 650°C and 750°C. The experimental data are given at 650°C. Here, the ratio C/N in the alloy is close to 1, and the nucleating particles are nitrogen-enriched and tend to the alloy stoichiometry only in the late coarsening stage.

### 3.4 Coupling nucleation and growth

Nucleation and growth are not successive stages, but are actually overlapping and hence are strongly coupled. In the mean field approximation, this coupling can be introduced mathematically through a nucleation and growth equation: during a heat treatment, the average radius  $r$  evolves not only due to growth of all existing precipitates,

but also due to the nucleation of new precipitates of radius  $r'$ . In terms of average growth rate, the coupling is simply additive and is rendered by the following equation [29]:

$$\left. \frac{dr}{dt} \right|_{\text{Nucl-Growth}} = \left. \frac{dr}{dt} \right|_{\text{Growth}} + \frac{1}{N} \frac{dN}{dt} (r' - r), \quad (27)$$

where the first term in the right-hand side is the growth rate of a precipitate of radius  $r$  and the second term is the effect of nucleation. In cases of isothermal heat treatments or moderate heating rates, this procedure has proved to be an excellent approximation relative to a Kampmann and Wagner numerical resolution or by comparison with more sophisticated models [62].

The coupling between nucleation and growth thus allows for describing the evolution of precipitation state of  $M(C_\gamma, N_{1-\gamma})$  in the ferritic matrix, as shown in Figure 12.

## 4 Conclusion

The present review highlights the difficulty of dealing with the nucleation and growth of tri-atomic and composition varying nanoprecipitates in the ferritic matrix. From a theoretical point of view, the mean field approach is a powerful method to describe quantitatively both the nucleation and the growth steps. More particularly, the results obtained, in terms of precipitate composition, allow a better understanding of the complex precipitation sequence: from a pure nitride to a carbo-nitride incorporating more and more carbons. However, as it stands, the present kinetics models do not take into account a number of involved phenomena. First, the heterogeneous nucleation of the carbo-nitride precipitates on defects such as dislocations in ferrite. In that precise case, the elastic interaction between dislocation and solute atoms could potentially modify the precipitation sequence. Second, the elastic strain energy associated to the formation of precipitates. The latter may modify the time evolution of carbo-nitrides composition, the nucleation and growth rate, and above all, the shape evolution of precipitates. Indeed, a non-negligible part of the elastic stress can be accommodated by crystal shape optimization, and a deviation from the Wulff shape, which minimizes surface energy, is thus expected during precipitation. However, it is known that plastic deformation, variant selection, and modification of equilibrium state are known as the mechanisms of stress relaxation. As a consequence, a competition among all the possible mechanisms of stress relaxation is expected. In such a case, the main question is through

which mechanisms does a system relax stresses and why? To our opinion, if this key question is not answered, it would be unrealistic to make a reliable prediction of both the coherency loss and the shape evolution.

## References

- [1] Ghosh A, Sahoo S, Ghosh M, Ghosh RN, Chakrabarti D. Effect of microstructural parameters, microtexture and matrix strain on the Charpy impact properties of low carbon HSLA steel containing MnS inclusions. *Mater. Sci. Eng. A* 2014, 613, 37–47.
- [2] Gladman T. *The physical metallurgy of microalloyed steel, book 615*. The Institute of Materials: London, 1999.
- [3] Song R, Ponge D, Raabe D, Speer JG, Matlock DK. Overview of processing, microstructure and mechanical properties of ultrafine grained bcc steels. *Mater. Sci. Eng. A* 2006, 441, 1–17.
- [4] Gouné M, Maugis P, Drillet J. Modelling of the interaction between phase transformation and precipitation: coupled kinetics in microalloyed multiphase steels. *Comput. Mater. Sci.* 2012, 55, 127–135.
- [5] Chen MY, Gouné M, Verdier M, Bréchet Y, Yang JR. Interphase precipitation in vanadium-alloyed steels: strengthening contribution and morphological variability with austenite to ferrite transformation. *Acta Mater.* 2014, 64, 78–92.
- [6] Isasti N, Jorge-Badiola D, Taheri ML, Uranga P. Microstructural features controlling mechanical properties in Nb-Mo microalloyed steels. Part I: yield strength. *Metall. Mater. Trans. A* 2014, 45, 4960–4971.
- [7] Chen J, Shen X, Ji F, Tang S, Liu Z, Wang G. Effect of annealing time on microstructure and mechanical properties of cold-rolled niobium and titanium bearing micro-alloyed steel strips. *J. Iron Steel Res. Int.* 2013, 20, 86–92.
- [8] Bu FZ, Wang XM, Yang SW, Shang CJ, Misra RDK. Contribution of interphase precipitation on yield strength in thermomechanically simulated Ti-Nb and Ti-Nb-Mo microalloyed steels. *Mater. Sci. Eng. A* 2015, 620, 22–29.
- [9] Palmiere EJ, Garcia CI, DeArdo AJ. The influence of niobium supersaturation in austenite on the static recrystallisation behaviour of low carbon microalloyed steels. *Metall. Mater. Trans. A* 1998, 27A-4, 951–960.
- [10] DeArdo AJ. Microalloyed strip steels for the 21st century. *Mater. Sci. Forum* 1998, 284–286, 15–26.
- [11] Charleux M, Poole WJ, Militzer M, Deschamps A. Precipitation behavior and its effect on strengthening of an HSLA-Nb/Ti steel. *Metall. Mater. Trans. A* 2001, 32, 1635–1647.
- [12] Ardell AJ. Precipitation hardening. *Metall. Trans. A* 1985, 16, 2131–2165.
- [13] Fossaert C, Rees G, Maurickx T, Bhadeshia HK. The effect of niobium on the hardenability of microalloyed austenite. *Metall. Mater. Trans. A* 1995, 26A, 21–30.
- [14] Ai JH, Zhao TC, Gao HJ, Hu YH, Xie XS. Effect of controlled rolling and cooling on the microstructure and mechanical properties of 60Si2MnA spring steel rod. *J. Mater. Process. Technol.* 2005, 160, 390–395.
- [15] Halfa H. Recent trends on producing ultrafine grained steels. *J. Miner. Mater. Character. Eng.* 2014, 2, 428–469.
- [16] Hofer F, Warbichler P, Buchmayr B, Kleber S. On the detection of MX precipitates in microalloyed steels using energy-filtering TEM. *J. Microsc.* 1996, 184–3, 163–174.
- [17] Craven AJ, He K, Garvie LA, Baker TN. Complex heterogeneous precipitation in Ti-Nb microalloyed Al-killed HSLA steels. *Acta Mater.* 2000, 48, 3857–3868.
- [18] Beres M, Weirich TE, Hulka K, Mayer J. TEM investigations of fine niobium precipitates in HSLA steel. *Steel Res. Int.* 2004, 75, 753–758.
- [19] Kampmann R, Wagner R. Homogeneous second phase precipitation. In *Materials Science and Technology: A Comprehensive Treatment*, vol. 5, Haasen P, Ed., VCH: Weinheim, 1991, pp. 213–304.
- [20] Liu WJ, Jonas JJ. Calculation of the Ti(Cy N1-y)-Ti4C2S2-MnS-austenite equilibrium in Ti-bearing steels. *Metall. Trans. A* 1989, 20, 1361–1374.
- [21] Dutta B, Sellars CM. Effect of composition and process variables on Nb(C,N) precipitation in niobium microalloyed austenite. *Mater. Sci. Technol.* 1987, 3, 197–206.
- [22] Liu WJ, Jonas JJ. Nucleation kinetics of Ti carbonitride in microalloyed austenite. *Metall. Trans. A* 1989, 20, 689–697.
- [23] Perez M, Deschamps A. Microscopic modelling of simultaneous two-phase precipitation: application to carbide precipitation in low-carbon steels. *Mater. Sci. Eng. A* 2003, 360, 214–219.
- [24] Maugis P, Gouné M. Kinetics of vanadium carbo-nitride precipitation in steel: a computer model. *Acta Mater.* 2005, 53, 3359–3367.
- [25] Perez M, Courtois E, Acevedo D, Epicier T, Maugis P. Precipitation of niobium carbonitrides in ferrite: chemical composition measurements and thermodynamic modelling. *Philos. Mag. Lett.* 2007, 87, 645–656.
- [26] Shercliff HR, Ashby MF. A process model for age hardening of aluminium alloys I and II. *Acta Metall. Mater.* 1990, 38, 1789–1812.
- [27] Deschamps A, Brechet Y. Influence of predeformation and ageing of an Al-Zn-Mg alloy: II. Modelling of precipitation kinetics and yield stress. *Acta Mater.* 1999, 47, 293–305.
- [28] Fujita N. Modelling carbide precipitation in alloy steels. PhD thesis. Department of Materials Science and Metallurgy, Cambridge University: Cambridge, 2000.
- [29] Gendt D, Maugis P, Bouaziz O, Lanteri S, Barges P. In *Mathematical Modeling in Metals Processing and Manufacturing*, Martin P, Ed., Metal Society: London, UK, 2000.
- [30] Gendt D. Cinétiques de précipitation du carbure de niobium dans la ferrite. PhD thesis. Orsay; 2001.
- [31] Rickerby DS, Henderson S, Hendry A, Jack KH. Structure and thermochemistry of nitrated iron-titanium alloys. *Acta Metall.* 1986, 34, 1687–1699.
- [32] Appolaire B, Gouné M. Linear stability analysis of a gamma  $\gamma'$ -Fe4N nitride layer growing in pure iron. *Comput. Mater. Sci.* 2006, 38, 126–135.
- [33] Van Landeghem HP, Gouné M, Redjaimia A. Nitride precipitation in compositionally heterogeneous alloys: nucleation, growth and coarsening during nitriding. *J. Cryst. Growth* 2012, 341, 53–60.
- [34] Jack DH, Jack KH. Carbides and nitrides in steels. *Mater. Sci. Eng.* 1973, 11, 1–27.
- [35] Mittemeijer EJ. Nitriding response of chromium-alloyed steels. *J. Met.* 1985, 37, 16–20.

- [36] Volmer M, Weber A. Keimbildung in Übersättigten Gebilden. *Z. Phys. Chem.* 1926 119, 277–301.
- [37] Farkas L. Keimbildungsgeschwindigkeit in Übersättigten Dämpfen. *Z. Phys. Chem.* 1927, 125, 239–242.
- [38] Becker R, Döring W. Kinetische Behandlung der Keimbildung in Übersättigten Dämpfen. *Ann. Phys.* 1935, 24, 719.
- [39] Aaronson HI, Lee JK. *Lectures on the Theory of Phase Transformations*, Aaronson HI, Ed., TMS-AIME: New York, 1982, pp. 83–115.
- [40] Russell KC. Linked flux analysis of nucleation in condensed phases. *Acta Metall.* 1968, 16, 761–769.
- [41] Christian JW. *The Theory of Transformations in Metals and Alloys Part 1*. Pergamon Press: Oxford, 2002, pp. 436–441.
- [42] Zeldovich JB. On the theory of new phase formation, cavitation. *Acta Phys-Chim. URSS* 1943, 18, 1–22.
- [43] Balluffi RW, Allen SM, Carter WC. *Kinetics of Materials*. John Wiley & Sons: Hoboken, 2005, pp. 459–499.
- [44] Appolaire B. Germination. Available at: [http://mms2.enscm.fr/mat\\_nancy/germination/transparents](http://mms2.enscm.fr/mat_nancy/germination/transparents). Accessed on 2010.
- [45] Hillert M. *Phase Equilibria-Phase Diagrams and Phase Transformations*. Cambridge University Press: Cambridge, 1998.
- [46] Samoilo A, Buchmagr B, Cerzak H. A thermodynamic model for composition and chemical driving force for nucleation of complex carbonitrides in microalloyed steel. *Steel Res.* 1994, 298–305.
- [47] Speer JG, Michael JR, Hansen SS. Carbonitride precipitation in niobium/vanadium microalloyed steels. *Metall. Trans. A* 1987, 18, 221.
- [48] Hillert M, Staffansson LI. The regular solution model for stoichiometric phases and ionic melts. *Acta Chem. Scand.* 1970, 24, 3618–3626.
- [49] Rios PR. Method for the determination of mole fraction and composition of a multicomponent fcc carbonitride. *Mater. Sci. Eng. A* 1991, 142, 87–94.
- [50] Rios P. Expression for solubility product of niobium carbonitride in austenite. *Mater. Sci. Technol.* 1988, 4, 324–327.
- [51] Lagneborg R, Siwecki T, Zajac S, Hutchinson B. The role of vanadium in microalloyed steels. Reprinted from *Scand. J. Metall.* 1999, 28, 1–241.
- [52] Scott CP, Drillet J. Quantitative analysis of local carbon concentration in TRIP steels. In *International Conference on TRIP-Aided High Strength Ferrous Alloys*. De Cooman BC, Ed., GRIPS: Bed Harzbourg, 2002, pp. 97–102.
- [53] Courtois E, Epicier T, Scott C. EELS study of niobium carbonitride nano-precipitates in ferrite. *Micron* 2006, 37, 5, 492–502.
- [54] Scott CP, Chaleix D, Barges P, Rebischung V. Quantitative analysis of complex carbo-nitride precipitates in steels. *Scripta Mater.* 2002, 47, 845–849.
- [55] Schmuck C, Auger P, Danoix F, Blavette D. Quantitative analysis of GP zones formed at room temperature in an 7150 Al-based alloy. *Appl. Surf. Sci.* 1995, 87/88, 228–233.
- [56] Danoix F, Epicier T, Vurpillot F, Blavette D. Atomic-scale imaging and analysis of single layer GP zones in a model steel. *J. Mater. Sci.* 2012, 47, 1567–1571.
- [57] Jack KH. The structure of nitride iron titanium alloys. *Acta Metall.* 1976, 24, 137–146.
- [58] Jessner P, Gouné M, Danoix R, Hannover B, Danoix F. Atom probe tomography evidence of nitrogen excess in the matrix of nitrided Fe-Cr. *Philos. Mag. Lett.* 2010, 90, 793–800.
- [59] Xie KY, Breen AJ, Yao L, Moody MP, Gault B, Cairney JM, Ringer SP. Overcoming challenges in the study of nitrided microalloyed steels using atom probe. *Ultramicroscopy* 2012, 112, 32–38.
- [60] Breen AJ; Xie KY, Moody MP, Gault B, Yen HW, Wong CC, Cairney JM, Ringer SP. *Microsc. Microanal.* 2014, 20, 1100–1110.
- [61] Noble B, Bray SE. Use of the Gibbs-Thompson relation to obtain the interfacial energy of  $\delta'$  precipitates in Al-Li alloys. *Mater. Sci. Eng. A* 1999, 266, 80–85.
- [62] Maugis P, Soisson F, Lae L. Kinetics of precipitation: comparison between Monte Carlo simulations, cluster dynamics and the classical theories. *Defect. Diffus. Forum* 2005, 237–240, 671–676.
- [63] Jang JH, Lee CH, Han HN, Bhadeshia HKDH, Suh DW. Modelling the coarsening behaviour of TiC precipitates in high-strength, low alloy steels. *Mater. Sci. Technol. SER* 2013, 29, 1074–1079.
- [64] Jang JH, Lee CH, Heo YU, Suh DW. Stability of (Ti, M)C (M=Nb, V, Mo and W) carbide in steels using first-principles calculations. *Acta Mater.* 2012, 60, 208–217.
- [65] Yamasaki S. Modelling precipitation of carbides in martensitic steels. PhD thesis, University of Cambridge: Cambridge, 2004.
- [66] Porter DA, Easterling KE. *Phase Transformations in Metals and Alloys*, 2nd ed. Chapman & Hall: London, 1992.
- [67] Yang ZG, Enomoto M. Discrete lattice plane analysis of Baker-Nutting related B1 compound/ferrite interfacial energy. *Mater. Sci. Eng. A* 2002, 332, 184–192.
- [68] Perrard F, Donnadieu P, Deschamps A, Barges P. TEM study of NbC heterogeneous precipitation in ferrite. *Philos. Mag.* 2006, 86, 4271–4284.
- [69] Teresiak A, Kubsch H. X-ray investigations of high energy ball milled transition metal carbides. *Nanostruct. Mater.* 1995, 6, 671–674.
- [70] Lipatnikov VN, Lengauer W, Ettmayer P, Keil E, Groboth G, Kny E. Effect of vacancy ordering on structure and properties of vanadium carbide. *J. Alloys Compd.* 1997, 261, 192–197.
- [71] Van Landeghem HP, Gouné M, Bordère S, Danoix F, Redjaïmia A. Competitive precipitation of amorphous and crystalline silicon nitride in ferrite: interaction between structure, morphology, and stress relaxation. *Acta Mater.* 2015, 93, 218–234.
- [72] Tingaud D, Maugis P. First-principles study of the stability of NbC and NbN precipitates under coherency strains in  $\alpha$ -iron. *Comput. Mater. Sci.* 2010, 49, 60–63.
- [73] Aaron HB, Fainstei D, Kotler GR. Diffusion-limited phase transformations – a comparative evaluation of mathematical approximations. *J. Appl. Phys.* 1970, 41, 4404–4410.
- [74] Zener C. Theory of growth of spherical precipitates from solid solution. *J. Appl. Phys.* 1949, 20, 950–953.
- [75] Thomson W (Lord Kelvin). On the equilibrium of vapour at a curved surface of liquid. *Philos. Mag.* 1871, 42, 448–452.
- [76] Gibbs JW. On the equilibrium of heterogeneous substances. *Am. J. Sci. Ser.* 1878, 3, 441–458.
- [77] Perez M, Dumont M, Acevedo-Reyes D. Implementation of classical nucleation and growth theories for precipitation. *Acta Mater.* 2008, 56, 2119–2132.
- [78] Rivera-Diaz-del-Castillo PEJ. Precipitate coarsening in multi-component systems. *Scripta Mater.* 2002, 47, 113–117.
- [79] Maugis P, Gouné M, Barges P, Dougnac D, Ravaine D, Lamberigts M, Siwecki T, Bi Y. A model for niobium carbonitride precipitation in ferrite. *Mater. Sci. Forum* 2003, 426–432, 1313–1318.



## Bionotes

### Mohamed Gouné

Institute for Condensed Matter and Chemistry of Bordeaux,  
CNRS UPR9048, 87 Avenue du Docteur Schweitzer,  
33608 Pessac cedex, France,  
[mm.goune@gmail.com](mailto:mm.goune@gmail.com)

Mohamed Gouné is a Full Professor at both Bordeaux University and the Institute for Condensed Matter and Chemistry of Bordeaux. He specializes in mesoscale modeling of precipitation and phase transformation in steels with a strong connection with experiments. He has supervised or co-supervised more than 10 PhDs dedicated to phase transformation in steels. He is in charge of many national and international projects and is involved in two international networks dedicated to phase transformations in solid state.

### Philippe Maugis

IM2NP, Aix-Marseille Université et Université de Toulon, UMR  
CNRS 7334, Faculté des Sciences et Techniques, Avenue Escadrille  
Normandie Niemen, 13397 Marseille Cedex 20, France

Philippe Maugis is a Full Professor at both University of Marseille and IM2NP. He worked for many years within the ArcelorMittal

research center in Maizières-Les-Metz as a researcher in the field of weldability and phase transformations in precipitation in steels. He is now the head of the research group at IM2NP. He is an internationally recognized specialist in multi-scale modeling of both phase transformations and precipitation in steels. He was involved in many national and international projects. He supervised and co-supervised many theses dedicated to physical metallurgy.

### Fredéric Danoix

GPM, Université et INSA de Rouen, UMR CNRS 6634, Normandie  
Université, UFR Sciences et Techniques,  
Avenue de l'Université, BP12, 76801 Saint Etienne du Rouvray,  
France

Fredéric Danoix is a researcher at GPM (University of Rouen). He is an internationally recognized specialist in 3D atom probe tomography, with extensive experience in the field of physical metallurgy. He supervised several PhD students in the same field. He is the coordinator of a national project, and he was involved in many international projects. He is currently responsible for the “structural materials” topics in the GPM research group ERAFEN.